Biomarkers reveal abrupt switches in hydroclimate during the last glacial in southern California

Sarah J. Feakins[a*], Mong Sin Wu [a], Camilo Ponton[a#], Jessica E. Tierney[c]

[a] *University of Southern California, Department of Earth Sciences, 3651 Trousdale Pkwy, Los Angeles, CA 90089-0740, USA*

[c]*University of Arizona, Department of Geosciences, 1040 E 4th St, Tucson, AZ 85721, USA*

*Corresponding author: feakins@usc.edu (Sarah Feakins)

[#] permanent address: *Western Washington University, Geology Department, 516 High Street, Bellingham, WA 98225*

Keywords: leaf wax; hydrogen isotope; GDGT; late Glacial; southern California

Abstract

Reconstructions of past hydroclimate provide a means to understand precipitation responses to global ocean-atmosphere climate dynamics beyond the scope of that in the instrumental record. Late glacial climate was characterized by abrupt variability in ice and ocean dynamics, however the implications for hydroclimate are not as well known. Here we present organic geochemical proxy evidence for precipitation isotopes based on plant leaf wax hydrogen isotopic compositions (δD_{wax}) and temperature proxy evidence based upon the branched glycerol dialkyl glycerol tetraethers (brGDGTs), that derive from the membrane lipids of bacteria, each extracted from a sedimentary archive in Lake Elsinore, California spanning 32 – 9 ka. We add proxy evidence for vegetation and salinity from additional biomarker analyses and compare to prior pollen and sedimentological evidence from the same core. Our record indicates a strong deglacial warming of 10°C in Lake Elsinore (beginning at 14.5 ka) that accompanied a D-enrichment of precipitation of +90‰ and more C_4 vegetation (12 – 10 ka), after a cold, wet and C_3-dominated phase (20 – 14.5 ka), indicating winter-dominated precipitation during the Last Glacial Maximum and Heinrich Stadial 1. During the late glacial (32 – 20 ka) we find abrupt variability, with precipitation isotopic shifts (~70‰) that are independent of temperature swings implicating changes in storm track, rather than local temperature as drivers of the precipitation isotope signal. Temperature is however not irrelevant for hydroclimate: we find extreme warmth at 29.4 ka and 26.8 ka, the latter coincident with existing reports of an extended dry period (27.5 – 25.5 ka), suggesting a long hot and dry interlude during the generally cooler glacial period. We compare δD_{wax} with speleothem $\delta^{18}O$ from Nevada, also within the winter-dominated precipitation region. Our results corroborate the Last Glacial Maximum and deglacial signals, and fill gaps revealing

storm-track instability from 32 – 20 ka, however the pacing and magnitude of the biomarker signals merit cautious interpretation.

1. Introduction

Southern California experiences substantial interannual variability in precipitation, with longer-duration hydroclimate shifts potentially leading to widespread drought and reduced water availability. Future climate projections suggest that southern California may be prone to more extreme drought under rising greenhouse gas concentrations, due to a combination of reduced precipitation and elevated temperatures (Williams et al., 2013). These concerns have motivated further study of the nature, magnitude and causes of hydroclimate variability in this subtropical, arid region both from climate modeling (Wei et al., 2016) and recent paleoclimate (tree-ring) perspectives (Griffin and Anchukaitis, 2014). Sedimentary records of hydroclimate provide a way to develop an even longer-term perspective on the range of variability that is possible for this region.

The isotopic composition of precipitation (oxygen and hydrogen) integrates the history of a water parcel in the atmosphere, including the source of moisture and rainout processes such as temperature of condensation and raindrop re-evaporation on descent (Dansgaard, 1964). In the coastal sector of the southwest US, storms sourced from tropical and subtropical North Pacific deliver more ^{18}O and D-enriched precipitation, whereas those sourced from the northern North Pacific are more depleted in the heavier isotope (Friedman et al., 1992). Trajectory analysis of individual storms reaching the southern Sierra Nevada during 2001 – 2005 finds that tropical storms have precipitation δD (δD_{precip}) values from −23 to −68‰ whereas north Pacific storms have values of −98 to −158‰ (Berkelhammer et al., 2012). Changes in storm tracks are related to the mean position and strength of the polar jet stream, steered by the location and intensity of the characteristic North Pacific high and Aleutian low-pressure cells. This pressure cell steering occurs in the present climate and also during the glacial climate, in the latter case associated with

pressure differences related to the cooling and topographic presence of the Cordilleran and Laurentide ice sheets (Oster et al., 2015a). Since precipitation isotopes reflect storm track direction, they offer proxy evidence for atmospheric circulation in the past, commonly reconstructed from speleothem archives of $\delta^{18}O$ (Asmerom et al., 2010; Wagner et al., 2010; Lachniet et al., 2014; Oster et al., 2015b).

Past δD_{precip} can be reconstructed using the hydrogen isotopic composition of the waxy molecules from plant leaves (δD_{wax}) that are well-preserved in sediments (Sachse et al., 2012). In California, the plant leaf wax *n*-alkanoic acids have been used as a proxy for δD_{precip} in marine sediments from the Santa Barbara Basin spanning 1.4 ka (Li et al., 2011); from Zaca Lake, spanning the last 3 ka (Feakins et al., 2014); and in a deglacial sequence, 19 – 13 ka, from Lake Elsinore (Kirby et al., 2013). Here we extend the Lake Elsinore reconstruction back to 32 ka, add sampling resolution across the deglacial and early Holocene interval, and integrate a late Holocene record from nearby Zaca Lake to provide a more complete history of precipitation isotope variability in southern California. We have constraints on the fidelity of the hydrogen isotopic composition of plant leaf wax *n*-alkanoic acids, δD_{wax}, as a recorder of δD_{precip} in the Lake Elsinore catchment from stream transported particulate organic matter (POM; this study), modern plant studies (Feakins and Sessions, 2010) and palynological reconstructions (Heusser et al., 2015). In addition, we measure the carbon isotopic composition of the plant wax molecules, $\delta^{13}C_{wax}$, in order to detect variations in aridity or a predicted increase in plants using the C_4 pathway during lower glacial atmospheric pCO_2, if temperatures were similar to or warmer than today, or if a change in precipitation seasonality led to water availability in the warmer months (Cotton et al., 2016).

We add an independent temperature reconstruction derived from another biomarker proxy, the brGDGT lipids, which allows us to evaluate the importance of temperature in driving hydroclimate variations. BrGDGTs derive from the membranes of bacteria that live in the surface waters of lakes as well as the soils in the surrounding catchment (Weijers et al., 2007; Tierney & Russell, 2009). The molecular structures have been shown to respond to temperature, a possible physiological response in order to maintain membrane fluidity (Weijers et al., 2007). Lake sediment calibrations of brGDGT indices show strong correlations with mean annual air temperature in a series of 65 East African lakes spanning 2 to 27 °C (Russell et al., 2018).

In addition, we analyze archaeol and the isoprenoidal GDGTs in order to measure the Archaeol and Caldarchaeol Ecometric (ACE) index (Turich and Freeman, 2011). The ACE index is the relative proportion of archaeol, a biomarker for hypersaline archaea, to caldarchaeol, a cosmopolitan isoGDGT that reflects Euryarchaeotal and Thaumarchaeotal inputs (Turich and Freeman, 2011). We use ACE as a qualitative proxy for salinity, that presumably tracks heightened evaporation relative to inputs and lake level decline. By employing both leaf wax and GDGT proxies, we are able to provide independent constraints on multiple components of hydroclimate – namely, the change in precipitation source as well as the balance of precipitation and evaporation.

2. Study Region

2.1. Lake Elsinore

Lake Elsinore (33.66 °N, 117.35 °W, 380 masl, Fig. 1) is the largest natural freshwater lake (25 km^2) in southern California (36 km inland). The modern lake is a closed basin with ~8 m water depth; overflow occurs when lake levels exceed 13 m depth (Kirby et al., 2013). Lake Elsinore is

fed by inflow from the ephemeral San Jacinto River (SJR) which originates in the San Jacinto Mountains (maximum elevation 3302 m) and drains a catchment of about 1870 km^2 (Fig. 1). Some minor additional discharge into the lake comes from surface runoff from the north slope of the Santa Ana Mountains, proximal to the lake. The flow of the SJR is highly episodic. Most runoff occurs during and following storm events a few days a year and during snowmelt from high elevations between January and April (U.S. Geological Survey, 2013). The mean discharge rate of the SJR is 0.46 $m^3 s^{-1}$, but flow can reach as high as 453 $m^3 s^{-1}$ as recorded in Feb 27, 1927 (U.S. Geological Survey, 2013). We sampled the SJR in this study to obtain an estimate of the integrated precipitation isotopes and leaf wax isotopic composition exported from the landscape towards the lake in the modern climate state.

2.2. Climate and vegetation

California experiences a winter-dominated precipitation seasonality with almost all precipitation falling between the months of October to May as westerly storm tracks from the Pacific (Cayan and Rhoads, 1984). Mean annual precipitation (MAP) in the Lake Elsinore catchment ranges from 300 mm yr^{-1} at lowland elevations (~400 – 700 masl, comprising >80% of the catchment area), to orographically enhanced precipitation (rain and snow) of 800 mm yr^{-1} at elevations >1500 masl on Mt. San Jacinto (PRISM Climate Group, Oregon State University, 2013). At lake level, mean annual temperature (MAT) averages 18°C, with summer average temperatures of 25°C, resulting in high potential evaporation rates and lake water loss of >1.4 m yr^{-1}(Kirby et al., 2013).

Vegetation in the lake catchment consists of sage scrub (*Artemisia*), and chaparral (*Ceanothus*) in the lowlands transitioning into scrub oak (*Quercus*) chaparral at mid elevations. Above ~1300

masl (Fig. 1C), full-stature oak and pine (*Pinus*) woodlands transitioning into open mixed conifer forests on the peaks of the San Jacinto Mountains above 2500 masl. Forest is sustained with the greater orographic precipitation at higher elevations and where snow cover is found in winter-months, as this provides infiltration rather than runoff, with the mean snowline at 2300 masl (Minnich, 1968).

3. Materials and methods

3.1. Sampling of river water and suspended sediment

River water samples were collected from three tributaries of the San Jacinto River, including above and below the chaparral to forest transition at 1300 masl (Fig. 1B and C) during an ephemeral flow event in the San Jacinto River on 27 Jan 2013 (peak flow ~0.5 $m^3 s^{-1}$). Samples were collected from the banks by immersing 20 L vessels into the stream. Suspended sediment >0.2 μm was collected on polyethylsulfone (PES) filters (147 mm diameter) within pressurized filter units (similar to the methods of Galy et al., 2011). Particulates were rinsed off the filter with milliQ water and freeze-dried to yield sediment samples. Water samples were collected into tightly capped glass vials for isotopic analysis.

3.2. Water isotopic analysis

δD and δ^{18}O values of river water were measured on 8 replicate injections of 1 μL water samples using a Los Gatos Research DLT-1000 liquid water isotope analyzer. Replicate measurements yielded a mean precision (1σ) of 0.3‰ (n = 24) and were calibrated using 3 working standards (Maui Water, δD = −10.6‰, δ^{18}O = −3.3‰; Caltech internal standard, δ D = −73.4‰, δ^{18}O =

147 −9.7‰; and LGR Water # 2, δD = −117.0‰, δ^{18}O = −15.5‰) to the VSMOW−SLAP isotopic
148 scale with accuracy better than 0.2‰ (δD) and 0.1‰ (δ^{18}O) respectively.

149 *3.3. Lake Elsinore sediment core*

150 Lake Elsinore sediment core LEDC10-1, extending from 9 to 30 m below lake floor, was
151 collected in 2010 as reported in Kirby et al. (2013a). Macrofossil radiocarbon dating and the
152 Bayesian software Bacon were used to develop an age model using 28 AMS radiocarbon dates.
153 (Heusser et al., 2015; Kirby et al., 2018). Radiocarbon uncertainties range from 35 years to 290
154 years with the largest calibration uncertainties between 13.4 and 16.1 ka BP. A lack of dated
155 macrofossils <10 ka and between 26.1 and 30.7 ka BP means that the uncertainty expands to >1
156 ka (Kirby et al., 2018). The core was subsampled every 30 cm (~ 400 yrs) for biomarker analyses
157 collecting samples spanning <2 cm (~25 yrs) with a metal tool. Our organic geochemical
158 analyses extend the record of δD_{wax} values reported for the deglacial as published in a regional
159 review (Kirby et al., 2013), and add to what is known from this core from pollen (Heusser et al.,
160 2015) and sedimentology (Kirby et al., 2018).

161 *3.4. Lipid extraction*

162 Sediment samples (5 g) were freeze-dried and homogenized. Sediments were solvent-extracted
163 with 9:1 v/v dichloromethane (DCM) to methanol (MeOH) at 100°C and 1500 psi for 30 minutes
164 using an Accelerated Solvent Extraction system (ASE 350®, Dionex). Total lipid extracts were
165 separated by column chromatography through LC-NH_2 gel into a neutral fraction and acid
166 fraction, using 2:1 DCM:isopropanol and 4% formic acid in diethyl ether respectively. The
167 neutral fraction contained the GDGTs and the acid fraction contained the *n*-alkanoic acids. The
168 acid fraction was methylated using MeOH of known isotopic composition in hydrochloric acid

169 (19:1 v/v) at 70°C for 12 h. The product was then diluted with milliQ water and partitioned into
170 hexane. The hexane fraction was then further separated over column chromatography through
171 silica gel (5% water-deactivated, 5 cm column) using hexane and DCM respectively. The DCM
172 fraction contained the *n*-alkanoic acid methyl esters.

173 *3.5. Plant wax n-alkanoic acid identification*

174 Compound identification and molecular abundance distribution of long chain *n*-alkanoic acid
175 methyl esters were determined by gas chromatography (Agilent 6890, for separation) mass
176 spectrometry (Agilent 5973, for compound identification) and flame ionization detection (for
177 quantification). Compound identification was based on mass spectra of target peaks compared to
178 library and retention time compared to standards. We calculated relative abundance of *n*-alkanoic
179 acids (C_{22} – C_{34}) from peak area response on the FID. We report the average chain length (ACL)
180 and carbon preference index (CPI):

181 $$ACL = \sum(n \times [C_n]) \quad \text{(Eq. 1)}$$

182 where n indicates the chain length (n = 22 – 34 for *n*-alkanoic acids), and $[C_n]$ indicates the
183 proportional abundance of that chain length, as well as:

184 $$CPI = ([C_{n-1}] + [C_{n+1}]) / 2\,[C_n] \quad \text{(Eq. 2)}$$

185 where n = 23 – 33 odd chains.

186 *3.6.Hydrogen isotopic analyses*

187 δD values of long chain *n*-alkanoic acid methyl esters were measured by a Thermo Scientific
188 Trace gas chromatograph connected to a Delta V Plus isotope ratio mass spectrometer via an

189 Isolink pyrolysis furnace at 1400°C. δD values were normalized to the Vienna Standard Mean
190 Ocean Water/Standard Light Antarctic Precipitation (VSMOW/SLAP) hydrogen isotopic scale
191 by comparing with an external standard (A5-Mix) containing 15 *n*-alkane compounds (C_{16} to C_{30})
192 obtained from A. Schimmelmann, Indiana University, Bloomington. The δD values of the
193 external standard mixture span −9 to −254‰. The RMS error of replicate measurements of the
194 standard was 3.2‰. An internal standard (C_{34} *n*-alkane) was co-injected with each sample to
195 check for stability throughout the sequence. The standard deviation of the internal standard was
196 3.6‰ across all analyses. δD values were then corrected for the δD of the added methyl group by
197 mass balance (δD of methanol = −198.3 ± 3.9‰, based on derivatization of phthalic acid of
198 known isotopic composition, and back calculating the δD of methanol). δD values were further
199 corrected for ice volume-related changes in ocean water isotopic composition, accounting for the
200 observations that the Last Glacial Maximum (LGM) ocean water was D-enriched by 8‰ relative
201 to today, with temporal variations scaled to the stacked benthic foraminiferal δ^{18}O record
202 (Lisiecki and Raymo, 2005). We report δD values of the C_{28} *n*-alkanoic acid as this homolog was
203 abundant in the core, is representative of terrestrial vegetation, and has been well-characterized
204 in our modern river and plant survey.

205 *3.7. Carbon isotopic analyses*

206 We also measured the δ^{13}C values of plant wax *n*-alkanoic acids. Analytical conditions were as
207 above except we used a combustion interface (instead of pyrolysis) at 1000°C. δ^{13}C values were
208 normalized to the Vienna Pee Dee Belemnite (VPDB/LVSEC) carbon isotopic scale using the
209 external standard mixture of C_{16} – C_{30} *n*-alkanes (A6-mix obtained from A. Schimmelmann,
210 Indiana University) whose δ^{13}C values span −26.2 to −33.8‰. The RMS error of replicate

211 measurements of the standard was 0.12‰. $\delta^{13}C$ values were corrected for the added methyl
212 group by mass balance ($\delta^{13}C$ of methanol = −25.45 ± 0.37 ‰, based on bulk measurement).

213 *3.8.GDGT analyses*

214 The neutral fractions were dissolved in hexane:isopropanol (99:1) and filtered through a 0.45
215 micron PTFE filter prior to injection on an Agilent 1260 High-Performance Liquid
216 Chromatography (HPLC) coupled to an Agilent 6120 mass spectrometer. Separation of the
217 GDGTs was accomplished using two BEH HILIC silica columns (2.1 x 150 mm, 1.7 um; Waters)
218 following the methods of Hopmans et al. (2016). Archaeol, the isoprenoidal GDGTs, and
219 branched GDGTs were detected in single ion monitoring mode, and quantified by comparison to
220 a C_{46} internal standard. The relative methylation of the 5' isomers of the brGDGTs is expressed
221 as the MBT'_{5Me} index (De Jonge et al., 2014),

222 $MBT'_{5Me} = (Ia + Ib + Ic) / (Ia + Ib + Ic + IIa + IIb + IIc + IIIa)$, (Eq. 3)

223 where the Type I, II and III brGDGTs have four, five, and six methyl groups respectively and the
224 Type a, b, and c brGDGTs has zero, one, and two rings, respectively. Duplicate analyses as well
225 as analyses of an internal laboratory standard throughout the runs yielded an error of 0.009
226 MBT'_{5Me} units (1-sigma).

227 To date, a global calibration of brGDGTs in lakes using the separation method of Hopmans et al.,
228 2016 does not yet exist, so to convert MBT'_{5Me} into temperature we apply the African lakes
229 calibration (Russell et al., 2018) using the equation:

230 $MAAT = 32.42 \times MBT'_{5me} - 1.21$ (Eq. 4)

231 with reported calibration RMSE of 2.4°C (n = 65, R^2 = 0.92).

232 We also calculated the index of two isoGDGT compounds, the Archaeol and Caldarchaeol
233 Ecometric (ACE) with the equation:

234 ACE = [archaeol]/[archaeol + caldarchaeol] x 100 (Eq. 5)

235 introduced as proxy for salinity (Turich and Freeman, 2011). Since we did not correct our
236 analyses for differential ionization of archaeol and caldarchaeol, we interpret the ACE index
237 exclusively in a qualitative sense (higher ACE = higher salinity). Duplicate analyses yielded an
238 average ACE error of 1.3 (1-sigma).

239 **4. Results and Discussion**

240 *4.1. Catchment constraints on plant wax as a proxy for δD_{precip}*

241 Normally the SJR is a dry river bed, however we captured a rare runoff event on 01/27/2013. We
242 found δD_w to be −73.7 ± 0.4‰ at 1630 masl in and −71.9 ± 1.1‰ at the lower elevation pair of
243 sites at 615 and 630 masl (Table 1). This is consistent with mean annual precipitation values of
244 −84 ‰ across 1982 − 1989 from 2540 masl (Friedman et al., 1992) and elevation trends of −10‰
245 km^{-1} (Williams and Rodoni, 1997). Two suspended sediment samples from the SJR at lower
246 elevations (~600 masl) yielded enough C_{28} *n*-alkanoic acid for isotopic analyses. δD_{wax} averages
247 −151 ± 5‰. The third sample at 1630 masl contains high concentrations of short-chains but low
248 abundance of long-chain (>C_{26}) *n*-alkanoic acids, likely due to the dominance of *Pinus* species,
249 which produce little *n*-alkanoic acids >C_{24} (Feakins et al., 2014). Thus, plant wax inputs to Lake
250 Elsinore are likely dominated by mid and low elevations, which also dominate the catchment by
251 area (Fig. 1).

Using the measured stream water and suspended sediment plant wax measured values, we calculate the net fractionation ($\varepsilon_{wax/w}$) using the equation:

$$\varepsilon_{wax/w} = [(\delta D_{wax} + 1) / (\delta D_w + 1) - 1] \quad \text{(Eq. 6)}$$

and obtain an $\varepsilon_{wax/w}$ of −86 ± 5‰ (1c.σ; Table 1). We do not suggest that the stream water is directly taken up by plants, but δD_w is similar to that of xylem water from plants in the catchment (Feakins and Sessions, 2010) in both cases reflecting an averaging of precipitation. Feakins and Sessions (2010) determined a weighted mean $\varepsilon_{wax/w}$ of −91 ± 23‰ for $C_{27\text{-}31}$ *n*-alkanes relative to xylem water for 9 species collected at 1620 masl within the SJR catchment, similar to fractionations found across southern California ($\varepsilon_{wax/w}$ = −94 ± 22‰;). About 300 km north in Zaca Lake, Feakins et al. (2014) determined a mean $\varepsilon_{wax/w}$ of −95 ± 22‰ for the C_{28} *n*-alkanoic acid compounds relative to precipitation from *Quercus*. $\varepsilon_{wax/w}$ are similar in the southern California region, and we use the SJR value here. For reference, SJR $\delta^{13}C_{wax}$ values average −32‰, consistent with C_3 vegetation and the lower values observed downcore during the late glacial. Relative abundance and central measure ACL = 26.1 are typical of those in the core, and CPI = 4.4 are consistent with the early Holocene values in the core (Appendix A).

3.9.Biomarker reconstructions and multiproxy comparison

The late glacial (32 – 20 cal. kyr BP) Lake Elsinore δD_{wax} record oscillates multiple times between ~−140‰ and −215‰ on multi-millennial time scales (Fig. 2A). While the mean values during late glacial are depleted relative to the early Holocene, the several abrupt δD_{wax} shifts of ~70‰ (between 32 and 20 ka) are comparable in magnitude to that of the deglacial sequence (~90‰). The molecular abundance distributions (ACL mean = 27.4 ± 0.7; CPI 5.5 ± 1.5,

Appendix A) show minimal variations, other than elevated CPI possibly associated with increased juniper or better preservation in cold and wet conditions. $\delta^{13}C_{wax}$ range from C_4 dominated, –18.1‰, to C_3 dominated –34.4‰ (mean = –28.1 ± 3.1‰, i.e., dominantly C_3, from n = 59 sediment core samples; Appendix A). We observe similar features in the $\delta^{13}C_{wax}$ and δD_{wax} (Fig. 2A) and a significant positive correlation (r = 0. 55, $p < 0.05$) determined by non-parametric methods that account for serial correlation (Ebisuzaki, 1997). We infer C_3 vegetation dominates during cold and wet conditions with winter-dominated precipitation and C_4 emerges in the warmth of the early Holocene.

The brGDGT record of lake temperatures indicates large temperature swings during the late glacial and deglacial (Fig. 2B). We use an East African calibration (Russell et al., 2018), and despite likely microbial community differences in California, the reconstructed temperatures are reasonable with early Holocene values close to modern (18˚C). The lowest temperature, 10˚C, occurs at 23.5 ka and the deglacial warming from 14 – 12 ka is >10˚C, agreeing with the pollen interpretations of ~11°C warming at the glacial termination (Heusser et al., 2015).

Temperatures >20°C are reported for six late glacial samples, including a high of 22°C at 29.4 ka and a maximum of 23˚C at 26.8 ka which coincides with the pollen-inferred warm and dry period from 27.5 – 25.5 ka (Heusser et al., 2015) when the lake was shallow (~3.2 – 4.5 m deep; Kirby et al., 2018). All evidence points to dry conditions caused by high temperatures and increased evaporation, though a shallower lake would experience greater seasonal temperature range and altered water column production, perhaps shifting from surface-dominated production (Loomis et al., 2014) to depth-integrated production (Weber et al., 2018). It is not clear what, if any, bias this would exert on temperature reconstructions relative to the deeper lake. As a cross-

check on variations in lake conditions, we investigated relative salinity changes with the ACE index. The ACE data show increases in salinity associated with elevated temperatures, representing a coherent record of increased temperature, evaporation and salinity (Fig. 2B). One exception is the low ACE in the sand layer (yellow shading; Fig. 2) that might reflect allochthonous (non-saline) inputs.

We see covariations between temperature and $\delta^{13}C_{wax}$ (Fig. 2, but the positive correlation is not significant r = 0.45, p = 0.07, calculated using the Ebisuzaki method). We find more ^{13}C-enriched values from 31 to 25 ka as well as from 11 to 10 ka, both warm times based on the brGDGT evidence. Warmer conditions in the low-pCO_2 glacial, could support an increase in C_4 vegetation in this region (Cotton et al., 2016). A ^{13}C enrichment from 24 – 22.5ka does not correspond to warmth, although it does correspond to D-enrichment, perhaps indicating summer precipitation, a variable known to support C_4 (Cotton et al., 2016).

After applying the local net fractionation ($\varepsilon_{wax/w}$ −86 ± 5‰) and correcting for glacial ice volume, we calculate δD_{precip} values between ~−50‰ and −130‰. The main uncertainties are changes in the plant community that may drive fractionation changes. Pollen reveals that glacial ecosystems differed from the modern with *Pinus* (not shown) and Cupressaceae (juniper, Fig. 2D) co-dominant through most of the late glacial and deglacial period, reflecting a descent of montane forest ecosystems by ~1000 m (Heusser et al., 2015). Between 27.5 – 25.5 ka dry taxa including Amaranthaceae, *Artemisia* and Asteraceae are abundant (Heusser et al., 2015). The transition to a modern ecosystem occurred between 14.4 to 10.8 ka when *Quercus* replaced Cupressaceae (Fig. 2) (Heusser et al., 2015). Grasses (Poaceae) were relatively constant and low (<10%) throughout the late glacial interval, with only one spike that reached 25% at ca. 25.5 ka BP (Heusser et al.,

317 2015). Aquatic pollen inputs comprise <5% of pollen (species including *Typha*, *Potamogeton* and
318 *Isoetes*), except for two pulses of 30% *Typha* at 31 and 25 ka, which are unlikely to reflect the
319 fractional input of plant waxes from species on the landscape. As downcore pollen variations are
320 not consistent with plant wax isotopic variations within the glacial, we infer that vegetation
321 changes do not substantially modulate the proxy, but there may be some amplification of the
322 deglacial precipitation isotope signal.

323 Based on calibration of the plant wax proxy with stem and leaf waters across the aridity gradient
324 in the region today (Feakins and Sessions, 2010), we do not anticipate much influence from
325 heightened soil evaporation in dry times. As noted in that study, woody vegetation in California
326 is adapted to the climate making use of winter precipitation by spring growth or deep roots and
327 episodic precipitation, via shallow roots. Soil evaporation occurs, but that D-enriched water is
328 scarce and not available to woody plants. Grasses, in contrast may see some soil water
329 evaporated signal (Smith and Freeman, 2006) however their fractionations are larger than those
330 of dicots (Sachse et al., 2012), so this effect may cancel out, and they have minor pollen
331 representation here. Neither do we expect variations in leaf water evaporation to lead to D-
332 enrichment in drier conditions as plants regulate water loss in water limiting conditions; for
333 example, Feakins and Sessions (2010) did not observe a sensitive response in leaf water between
334 coast and inland along an aridity gradient.

335 Each reported measurement represents a multidecadal mean, and we see values that are slightly
336 more positive (more southwesterly moisture and/or drier) and more negative than today (much
337 more northerly, colder or wetter). Given the D-enrichment at 27 ka occurs at a time identified as
338 dry, it seems like drought may contribute modestly to the signal, perhaps most likely due to the

process of rain-drop re-evaporation on descent through a dry atmosphere, rather than soil/leaf evaporation for the reasons noted above, or there may have been a slightly greater proportion of southwesterly storm tracks, although dry conditions prevailed. Between 25 and 19 ka during the glacial we see variability, with peaks at around 24 to 23 and around 20 ka when D-enriched values occur during the glacial maximum. Otherwise we see deviations to much more negative values than modern, in the glacial record from 19 – 15 ka in line with expectations from other records. More D-depleted precipitation can be produced by a greater amount of precipitation, a higher elevation of condensation or colder condensation temperature and a more northerly moisture source. Reconstructed δD_{precip} of −130 ‰ is therefore consistent with cold, distilled moisture from strong westerly flow to this location.

Evidence for wetter conditions comes from low salinity (Fig 2B), low proportions of xeric taxa, increased proportions of juniper-types (Fig. 2C) and increased sand-sized grains in the core as evidence for increased runoff (Kirby et al., 2018; Fig 2D). Based on these multi-proxy lines of evidence we find wetter conditions from 25 – 15 ka (blue shading, Fig. 2) especially during 20 – 15 ka. These are also cooler years as evidenced by the brGDGTs (Fig. 2B). Conversely, we see generally drier conditions associated with warmer temperatures in the remainder of the record, confirming the dominant role for temperature in modulating precipitation-evaporation patterns.

Following the cold and wet interlude, we see both deglacial warming and D-enrichment occurring abruptly after 15 ka, but with different timing such that the brGDGTs and δD_{wax} are not significantly correlated. This observation is consistent with old ideas about the displacement of storm tracks around the retreating Laurentide ice sheet. One study suggests more sinusoidal (northerlies) in LGM simulations (Oster et al., 2015a) with more zonal (westerlies) after the

deglaciation, in the Bølling simulation (14 ka) (Wong et al., 2016). However, most dynamical studies suggest a southward displacement of the jet stream in zonal configuration during the LGM relative to the modern tilted orientation (e.g. Löfverström and Lora, 2017). An alternate hypothesis proposes an increase in Atmospheric Rivers, as suggested by Lyle et al., (2012) and represented in model experiments (Lora et al., 2017), with support from time-transient lake highstands (McGee et al., 2018). However southerly moisture carries a clear D-enriched signal integrated across AR landfalling events (Coplen et al., 2008) and we find no support for more southerly D-enriched precipitation during the LGM. Instead cold, northwesterly or westerly moisture advection during the LGM could explain D-depletion.

The divergence between temperature and δD during the remainder of the record further support a storm-track explanation. From 13 – 11 ka the records diverge, brGDGT temperatures dip by ~2˚C from 11.5 – 10.8 ka, following a plateau in the precipitation isotopes (Fig. 2), neither of which demonstrate a clear response to the Younger Dryas. During the late glacial period (33 – 20 ka), there is no coherence between the δD and temperature oscillations, which further implies that δD_{precip} is primarily controlled by changes in circulation (and not changes in temperature of condensation or other local effects).

3.10. Paleoprecipitation isotope intercomparison

The late glacial (32 – 20 cal. kyr BP) Lake Elsinore δD_{wax} record indicates large, millennial-scale abrupt fluctuations in hydroclimate (Fig. 2), with δD_{precip} values estimated to shift at times abruptly between ~−50‰ and −130‰ (Fig. 3). As this is not the first plant wax reconstruction in the southwest, we can compare values to proxy archives in the region, all reporting the same C_{28} *n*-alkanoic acid. We find the Lake Elsinore early Holocene (9 – 8 kyr BP) values are slightly

elevated above those for the late Holocene (3.5 – 0 ka) from Zaca Lake, NW of this site, near Santa Barbara, California (Feakins et al., 2104; Fig. 3) and a 1.4 – 0 ka marine record offshore in the Santa Barbara Basin (Li et al., 2011; not shown). A Holocene trend towards more depleted values has also been observed in the speleothem $\delta^{18}O$ from Nevada (Fig. 3). This trend has been linked to a change in summer insolation (Lachniet et al., 2014), however the mechanisms linking summer insolation to water isotopes are unclear given that the region experiences a winter-dominated precipitation regime.

Across the deglacial (15 – 10 ka), the Lake Elsinore reconstructed δD_{precip} shows a steady trend towards higher values (Kirby et al., 2013). As noted previously (Kirby et al., 2013; Oster et al., 2015b), Lake Elsinore δD_{wax} shows a muted response to the Younger Dryas event unlike speleothem records from Moaning Cave, Sierra Nevada, California (Oster et al., 2015b) and speleothems in the North American Monsoon region (New Mexico and Arizona) that show a $\delta^{18}O$ dip of 1‰ equivalent to half the deglacial signal (Asmerom et al., 2010; Wagner et al., 2010) as well as Leviathan Cave, Nevada (Lachniet et al., 2014). These records suggest that the Younger Dryas was a modest hydroclimate perturbation in much of California and Nevada, though amplified at high altitude or with temperature effects within caves.

The extended Lake Elsinore δD_{wax} record now allows us to consider variability in the late glacial (back to 33 ka) and allows us to fill gaps in regional hydroclimate history (Fig. 3). A composite cave record spanning 2 glacial cycles from Leviathan, Pinnacle and Lehman Caves, Nevada has a hiatus from 32 – 13 ka, a gap that has been partially filled with a record from Pinnacle Cave, Nevada spanning 20 – 16 ka, and extended from 105 – 175 ka with Lehman Cave to form the

404 "Leviathan Chronology" (i.e. the composite of Leviathan, Lehman and Pinnacle Caves in
405 Nevada; Lachniet et al., 2014, Lachniet 2016).

406 Both the Elsinore and Leviathan records reveal analogous deglacial enrichments in the heavier
407 isotope, although the magnitude of the transition is larger in the plant wax archive, even after
408 scaling for mass dependent fractionations which are 8x larger for D/H than for $^{18}O/^{16}O$ (Fig. 3).
409 The LGM component of the Leviathan Chronology includes adjustment of the Pinnacle Cave
410 record $\delta^{18}O_{calcite\text{-}VPDB}$ by –3‰ to account for spatial differences between the two cave sites
411 (Lachniet et al., 2014). Our study corroborates the direction of calcite adjustment and further
412 suggests the precipitation isotopic offset may have been even larger between the LGM and
413 Holocene. It is not clear whether the difference reflects spatial differences in climate between
414 Nevada and California; changing plant wax fractionation ($\varepsilon_{wax/w}$) associated with relative
415 humidity and vegetation change; or whether karstic processes (e.g., temperature of calcite
416 precipitation, off-gassing rates, flow-paths and times) are attenuating the amplitude of the
417 precipitation isotopic composition captured by the cave calcite $\delta^{18}O$ signals (Lachniet, 2009). If
418 cooler temperatures suppressed the magnitude of the cave recorded signal, and if vegetation
419 amplified that of plant wax, then the two approaches offer a complementary pairing to assess
420 precipitation isotopes across large Pleistocene swings in temperature.

421 Cave and lake records corroborate that precipitation during the LGM and Heinrich Stadial 1 (20
422 – 14.5 ka), was depleted in the heavier isotopes, when other proxies indicate wet conditions.
423 There are two alternate dynamical explanations for the pluvial. The first invokes increased
424 summer, southerly-derived precipitation associated with Atmospheric Rivers (Lyle et al., 2012,
425 Lora et al., 2017, McGee et al., 2018). We do not find the summer precipitation hypothesis to be

supported by proxy cave and plant wax evidence for ^{18}O or D-depleted precipitation. Another study of δD_{wax} from the Gulf of California, within in the North American Monsoon influenced region, also found weakened summer moisture inflow while the LIS was present (Bhattacharya et al., 2017). In addition, we find C_3-dominated vegetation, suggesting winter-season precipitation dominated in the Elsinore catchment during the LGM, like today. A second hypothesis invokes a glacial climate with more D-depleted wintertime precipitation from westerly or northwesterly sources, with greater antecedent rainout and colder temperatures driving D-depletion (Oster et al., 2015a, Löfverström and Lora, 2017). This hypothesis is consistent with the cave records and δD_{wax}. Lake Elsinore is within the winter-dominated precipitation zone today and apparently even more so during the LGM (D-depleted rainfall, dominance of C_3 plants). Our record spans critical gaps in the Leviathan Chronology and helps to constrain the duration of this D-depleted LGM-type hydroclimate mode. We find that 20 ka was the start of the most D-depleted precipitation at the LGM, and that the deglacial D-enrichment began abruptly at 15 ka.

During the late glacial (32 – 20 ka), Lake Elsinore fills another gap in the Leviathan Chronology, and reveals large magnitude variability of ~70‰. This is equivalent to the difference observed between modern northern and tropical North Pacific-sourced storms reaching the southern Sierra Nevada (~80‰; Berkelhammer et al., 2012). Based on the prior discussion, we suggest that storm track shifts are the likely explanation, although we note that end-member δD_{precip} characteristics from northern and tropical moisture sources likely differed between Holocene and glacial times (e.g. due to changes in SST, prior rainout, temperature of condensation and raindrop re-evaporation). Isotope-enabled climate model experiments find consistently more D- or ^{18}O-depleted precipitation during the late glacial in the southwest North America suggesting greater

449 upstream distillation during the late glacial than under modern climate (Jasechko et al., 2015).
450 While the model simulations differ in their spatial distribution of the boundary of this D- or ^{18}O-
451 depleted precipitation zone, and the model resolution is insufficient to capture catchment scale
452 features relevant here, we note they generally indicate relatively little change in the isotopic
453 composition of precipitation near the coastal region in which Lake Elsinore lies. Jasechko et al.,
454 (2015) further suggest that there is a larger amplitude isotope distillation effect at high latitudes
455 and inland in the context of the steeper equator-to-pole temperature gradient of glacial climate
456 compared to today.

457 What then ultimately drives late glacial variability in Lake Elsinore paleoprecipitation isotopes
458 remains unclear. We do not find clear association between abrupt variability in high latitudes (e.g.
459 the Greenland archive shown in Fig. 4) and the variability in Lake Elsinore across 32 – 20 ka,
460 which may reflect dating or proxy uncertainties, a lack of a causal connection or insufficient
461 length record to make secure determinations.

462 *3.11. Comparison to SSTs in the Santa Barbara Basin*

463 Other evidence for late glacial climate variability in southern California, comes from high
464 resolution sea surface temperature (SST) archives available nearby from the Santa Barbara Basin
465 (SBB). We compare alkenone-based reconstructions (Seki et al., 2002) as well as Mg/Ca of the
466 planktic foraminifera species *Globigerinoides bulloides* (Pak et al., 2012) from the SBB, which
467 both show SST variability within the last glacial and a deglacial warming, each with some
468 similarities and differences to the Lake Elsinore record (Fig. 4). Differences may relate to greater
469 advection of alkenones relative to foraminifera, or seasonal or depth-based differences in growth

habitat. The narrow temperature preference for the coccolithophores may damp the alkenone variability relative to *G. bulloides* that grows year-round in the modern system (Pak et al., 2012).

Comparing Lake Elsinore temperatures and SST estimates from the SBB (Fig. 4) we find lake temperatures are almost always warmer than ocean temperatures by up to 10°C during peak warm conditions at 29, 27, 13 and 10 ka. The anomalous lake warmth finds local corroboration in pollen records, that also differ between archives (Heusser et al., 2015). Land-sea temperature differences are more commonly about 5°C and sometimes within 1 – 2°C, such as at 31, 25 and 15 ka. The deglacial temperature rise is similar in magnitude at least between the Mg/Ca and brGDGT records, although it differs in timing, with the marine records warming early (~18 ka) and being more gradual (with Mg/Ca warmer than alkenones across 15 – 10 ka), whereas Lake Elsinore shows a large jump in temperatures similar to, but following, the abrupt transition at the start of the Bölling-Allerød (BA; Fig. 4). Between the BA and the previous interstadial, cool temperatures are seen in the Lake Elsinore, the SBB and the Greenland records reflecting the global cooling associated with ice expansion across northern North America during the Last Glacial Maximum. Several interstadials (interstadials 6 – 3; Fig 5) interrupt conditions on Greenland between 34 and 27 ka, but these are short-lived features. In contrast, we find a sustained strong warming (> 15°C representing a +5 °C jump over prior conditions) between 31 and 24 ka in the lake brGDGT data, with two maxima of 22°C at 29.4 ka and 23˚C at 26.8 ka. The warmth at 26.8 ka also corresponds to dry conditions, with a shallow lake and these may be interrelated: either, the shallower lake may have warmed considerably (but one would expect greater seasonality rather than just warming), alternatively the extreme warming may have led to drying and shrinking of the lake. ACE data (Fig. 2) indicates a saltier lake for much of 32 – 23 ka.

492 Those locally warmer temperatures, during times of globally low pCO_2, may explain the
493 observation of increased C_4 vegetation here.

494 **4. Conclusions**

495 In this study, we take a multi-biomarker approach to investigate late glacial climate variability
496 from the sediments of Lake Elsinore, southern California. We reconstruct the isotopic
497 composition of precipitation based upon the plant wax proxy (δD_{wax}) and infer vegetation
498 changes from $\delta^{13}C_{wax}$. We reconstruct temperatures from distributions of the brGDGT
499 compounds (MBT'_{5me}) and salinity variations from ACE. The deglacial transition in δD_{wax}
500 matches the timing of that in the Leviathan Chronology, a speleothem archive of oxygen isotopes
501 in precipitation (Lachniet et al., 2014), although the amplitude of the plant wax signal is larger
502 that of the cave deposits.

503 Temperatures warm with similar timing to the precipitation isotope and a C_4 vegetation increase
504 at the deglacial, suggesting warming, drying and a shift in storm tracks. We find lake
505 temperatures rise by 10°C at the deglacial transition confirming estimates based on pollen
506 (Heusser et al., 2015). Overall temperatures do not covary with precipitation isotope shifts in the
507 longer record. Instead our isotope results are consistent with dynamical reorganization of
508 atmospheric circulation that link D-depleted moisture with the southward displacement of storm
509 tracks during peak LIS extent. C_3 vegetation confirms winter-dominated precipitation in this cold
510 and wet phase. Our extended record also reveals precipitation isotopic instability during the late
511 glacial, filling a gap from 32 – 20 ka in the late glacial Leviathan Chronology. During this time,
512 we find that δD_{precip} shifted by as much as ~70‰. This late glacial precipitation isotope
513 variability is independent of temperature shifts. Lake temperature shifts show some similarity to

514 temperature estimates from the Santa Barbara Basin. Within the late glacial from 31 to 25 ka
515 warm SSTs in the SBB are accompanied by additional warming on land, with lake temperatures
516 equivalent to those of the early Holocene with commensurate changes in salinity reflecting
517 reduced water balance changes, and a slight increase in water stressed or C_4 vegetation. We find
518 an interval of extreme warmth in Lake Elsinore, ca. 27 ka, associated with prolonged dry
519 conditions, that implicates temperature, independent from atmospheric circulation, as a factor in
520 extreme, extended drought in southern California.

521 **Acknowledgements**

522 This study was supported by U.S. National Science Foundation Grant 1203549 to SF and the
523 David and Lucile Packard Foundation Fellowship to JT. We thank Matthew Kirby and Linda
524 Heusser for collaboration in an earlier phase of the project. We thank Alex Sessions for access to
525 the Los Gatos water isotope analyzer at the California Institute of Technology; Miguel Rincon
526 for laboratory assistance; and Josh West for field assistance with river sampling.

527 **Appendix A. Supplementary data**

528 Supplementary data associated with this article can be found in the online version at
529 http://dx.doi.org/10.....

530 **References**

531 Asmerom, Y., Polyak, V.J., Burns, S.J., 2010. Variable winter moisture in the southwestern
532 United States linked to rapid glacial climate shifts. Nat. Geosci. 3, 114-117.
533 Berkelhammer, M., Stott, L., Yoshimura, K., Johnson, K., Sinha, A., 2012. Synoptic and
534 mesoscale controls on the isotopic composition of precipitation in the western United
535 States. Clim. Dyn. 38, 433-454.

536 Bhattacharya, T., Tierney, J.E., Addison, J.A., Murray, J.W., 2018. Ice-sheet modulation of
537 deglacial North American monsoon intensification. Nat. Geosci. 11, 848-852
538 Cayan, D.R., Rhoads, J., 1984. Local relationships between United States west coast
539 precipitation and monthly mean circulation parameters. Mon. Weather Rev. 112, 1276-
540 1282.
541 Cotton, J.M., Cerling, T.E., Hoppe, K.A., Mosier, T.M., Still, C.J., 2016. Climate, CO_2, and the
542 history of North American grasses since the Last Glacial Maximum. Sci. Adv. 2,
543 e1501346.
544 Dansgaard, W., 1964. Stable isotopes in precipitation. Tellus 16, 436-468.
545 De Jonge, C., Hopmans, E.C., Zell, C.I., Kim, J.H., Schouten, S., Damste, J.S.S., 2014.
546 Occurrence and abundance of 6-methyl branched glycerol dialkyl glycerol tetraethers in
547 soils: Implications for palaeoclimate reconstruction. Geochim. Cosmochim. Acta 141,
548 97-112.
549 Ebisuzaki, W, 1997: A method to estimate the statistical significance of a correlation when the
550 data are serially correlated. J. Clim. 10, 2147-2153.
551 Feakins, S., Sessions, A.L., 2010. Controls on the D/H ratios of plant leaf waxes from an arid
552 ecosystem. Geochim. Cosmochim. Acta 74, 2128-2141.
553 Feakins, S.J., Kirby, M.E., Cheetham, M.I., Ibarra, Y., Zimmerman, S.R.H., 2014. Fluctuation in
554 leaf wax D/H ratio from a southern California lake records significant variability in
555 isotopes in precipitation during the late Holocene. Org. Geochem. 66, 48-59.
556 Friedman, I., Smith, G.I., Gleason, J.D., Warden, A., Harris, J.M., 1992. Stable isotope
557 composition of waters in southeastern California .1. Modern Precipitation. J. Geophys.
558 Res. 97, 5795-5812.

559 Galy, V., Eglinton, T., France-Lanord, C., Sylva, S., 2011. The provenance of vegetation and
560 environmental signatures encoded in vascular plant biomarkers carried by the Ganges-
561 Brahmaputra rivers. Earth Planet. Sci. Lett. 304, 1-12.
562 Griffin, D., Anchukaitis, K.J., 2014. How unusual is the 2012-2014 California drought? Geophys.
563 Res. Lett., 2014GL062433.
564 Heusser, L.E., Kirby, M.E., Nichols, J.E., 2015. Pollen-based evidence of extreme drought
565 during the last Glacial (32.6–9.0 ka) in coastal southern California. Quat. Sci. Rev. 126,
566 242-253.
567 Hopmans, E.C., Schouten, S., Sinninghe Damsté, J.S., 2016. The effect of improved
568 chromatography on GDGT-based palaeoproxies. Org. Geochem. 93, 1-6.
569 Jasechko, S., Lechler, A., Pausata, F.S.R., Fawcett, P.J., Gleeson, T., Cendón, D.I., Galewsky, J.,
570 LeGrande, A.N., Risi, C., Sharp, Z.D., Welker, J.M., Werner, M., Yoshimura, K., 2015.
571 Late-glacial to late-Holocene shifts in global precipitation δ18O. Clim. Past 11, 1375-
572 1393.
573 Kirby, M., Feakins, S.J., Bonuso, N., Fantozzi, J., Hiner, C., 2013. Latest Pleistocene to
574 Holocene hydroclimates from Lake Elsinore, California. Quat. Sci. Rev. 76, 1-15.
575 Kirby, M.E., Heusser, L., Scholz, C., Ramezan, R., Anderson, M.A., Markle, B., Rhodes, E.,
576 Glover, K.C., Fantozzi, J., Hiner, C., Price, B., Rangel, H., 2018. A late Wisconsin (32–
577 10k cal a BP) history of pluvials, droughts and vegetation in the Pacific south-west
578 United States (Lake Elsinore, CA). J. Quat. Sci. 33, 238-254.
579 Lachniet, M.S., 2009. Climatic and environmental controls on speleothem oxygen-isotope values.
580 Quat. Sci. Rev. 28, 412-432.

581 Lachniet, M.S., Denniston, R.F., Asmerom, Y., Polyak, V.J., 2014. Orbital control of western
582 North America atmospheric circulation and climate over two glacial cycles. Nat.
583 Commun. 5, doi:10.1038/ncomms4805.
584 Lachniet, M.S., 2016. Chapter 20 - A Speleothem Record of Great Basin Paleoclimate: The
585 Leviathan Chronology, Nevada, in: Oviatt, C.G., Shroder, J.F. (Eds.), Dev. Earth Surf.
586 Process. Elsevier, pp. 551-569.
587 Li, C., Sessions, A.L., Valentine, D.L., Thiagarajan, N., 2011. D/H variation in terrestrial lipids
588 from Santa Barbara Basin over the past 1400 years: A preliminary assessment of
589 paleoclimatic relevance. Org. Geochem. 42, 15-24.
590 Lisiecki, L., Raymo, M., 2005. A Pliocene-Pleistocene stack of 57 globally distributed benthic
591 $\delta^{18}O$ records. Paleocean. 20, 1-17.
592 Loomis, S.E., Russell, J.M., Ladd, B., Street-Perrott, F.A., Sinninghe Damsté, J.S., 2012.
593 Calibration and application of the branched GDGT temperature proxy on East African
594 lake sediments. Earth Planet. Sci. Lett. 357-358, 277-288.
595 Loomis, S.E., Russell, J.M., Heureux, A.M., D'Andrea, W.J., Sinninghe Damsté, J.S., 2014.
596 Seasonal variability of branched glycerol dialkyl glycerol tetraethers (brGDGTs) in a
597 temperate lake system. Geochim. Cosmochim. Acta. 144, 173-187.
598 Löfverström, M., Lora, J.M., 2017. Abrupt regime shifts in the North Atlantic atmospheric
599 circulation over the last deglaciation. Geophys. Res. Lett. 44, 8047-8055.
600 Lora, J.M., Mitchell, J.L., Risi, C., Tripati, A.E., 2017. North Pacific atmospheric rivers and their
601 influence on western North America at the Last Glacial Maximum. Geophys. Res. Lett.
602 44, 1051-1059.

603 Lyle, M., Heusser, L., Ravelo, C., Yamamoto, M., Barron, J., Diffenbaugh, N.S., Herbert, T.,
604 Andreasen, D., 2012. Out of the Tropics: The Pacific, Great Basin Lakes, and Late
605 Pleistocene Water Cycle in the Western United States. Science 337, 1629-1633.
606 Minnich, R.A., 1986. Snow levels and amounts in the mountains of southern California. J.
607 Hydrol. 89, 37-58.
608 Monnin, E., Indermuhle, A., Dallenbach, A., Fluckiger, J., Stauffer, B., Stocker, T.F., Raynaud,
609 D., Barnola, J.-M. 2001. Atmospheric CO_2 concentrations over the last glacial
610 termination. Science, 291, 112-114.
611 North Greenland Ice Core Project members, 2004. High-resolution record of Northern
612 Hemisphere climate extending into the last interglacial period. Nature 431, 147,
613 doi:10.1038/nature02805.
614 Oster, J.L., Ibarra, D.E., Winnick, M.J., Maher, K., 2015a. Steering of westerly storms over
615 western North America at the Last Glacial Maximum. Nat. Geosci. 8, 201-205.
616 Oster, J.L., Montanez, I.P., Santare, L.R., Sharp, W.D., Wong, C., Cooper, K.M., 2015b.
617 Stalagmite records of hydroclimate in central California during termination 1. Quat. Sci.
618 Rev. 127, 199-214.
619 Oster, J.L., Montañez, I.P., Sharp, W.D., Cooper, K.M., 2009. Late Pleistocene California
620 droughts during deglaciation and Arctic warming. Earth Planet. Sci. Lett 288, 434-443.
621 Pak, D.K., Lea, D.W., Kennett, J.P., 2012. Millennial scale changes in sea surface temperature
622 and ocean circulation in the northeast Pacific, 10–60 kyr BP. Paleocean. 27,
623 doi:10.1029/2011PA002238.
624 Petit, J.R., Jouzel, J., Raynaud, D., Barkov, N.I., Barnola, J.-M., Basile, I., Bender, M.,
625 Chappellaz, J., Davis, M. Delayque, G. Delmotte, M. Kotlyakov, V.M. Legrand, M.

626 Lipenkov, V.Y., Lorius, C., Pepin, L., Ritz, C. Saltzman, E., Stievenard, M. 1999. Climate
627 and atmospheric history of the past 420,000 years from the Vostok ice core, Antarctica.
628 Nature. 399, 429-436.

629 Russell, J.M., Hopmans, E.C., Loomis, S.E., Liang, J., Sinninghe Damsté, J.S., 2018.
630 Distributions of 5- and 6-methyl branched glycerol dialkyl glycerol tetraethers (brGDGTs)
631 in East African lake sediment: Effects of temperature, pH, and new lacustrine
632 paleotemperature calibrations. Org. Geochem. 117, 56-69.
633 Sachse, D., Billault, I., Bowen, G.J., Chikaraishi, Y., Dawson, T.E., Feakins, S.J., Freeman, K.H.,
634 Magill, C.R., McInerney, F.A., van der Meer, M.T.J., Polissar, P., Robins, R.J., Sachs,
635 J.P., Schmidt, H.-L., Sessions, A.L., White, J.W.C., West, J.B., Kahmen, A., 2012.
636 Molecular Paleohydrology: Interpreting the Hydrogen-Isotopic Composition of Lipid
637 Biomarkers from Photosynthesizing Organisms. Ann. Rev. Earth Planet. Sci. 40, 221-249.
638 Seki, O., Ishiwatari, R., Matsumoto, K., 2002. Millennial climate oscillations in NE Pacific
639 surface waters over the last 82 kyr: New evidence from alkenones. Geophys. Res. Lett.
640 29, 59-1-59-4.
641 Smith, F., Freeman, K., 2006. Influence of physiology and climate on δD of leaf wax *n*-alkanes
642 from C_3 and C_4 grasses. Geochim. Cosmochim. Acta 70, 1172-1187.
643 Tierney, J.E. and Russell, J.M., 2009. Distributions of branched GDGTs in a tropical lake system:
644 implications for lacustrine application of the MBT/CBT paleoproxy. Org. Geochem., 40,
645 1032-1036.
646 Turich, C., Freeman, K.H., 2011. Archaeal lipids record paleosalinity in hypersaline systems.
647 Org. Geochem. 42, 1147-1157.

Wagner, J.D.M., Cole, J.E., Beck, J.W., Patchett, P.J., Henderson, G.M., Barnett, H.R., 2010. Moisture variability in the southwestern United States linked to abrupt glacial climate change. Nat. Geosci. 3, 110, doi: 10.1038/ngeo707.

Weber, Y., Damsté, J.S.S., Zopfi, J., De Jonge, C., Gilli, A., Schubert, C.J., Lepori, F., Lehmann, M.F. and Niemann, H., 2018. Redox-dependent niche differentiation provides evidence for multiple bacterial sources of glycerol tetraether lipids in lakes. Proc. Natl. Acad. Sci. U.S.A. 115, 0926-10931

Wei, J., Jin, Q., Yang, Z.-L., Dirmeyer, P.A., 2016. Role of ocean evaporation in California droughts and floods. Geophys. Res. Lett., doi:10.1002/2016GL069386.

Weijers, J.W., Schouten, S., van den Donker, J.C., Hopmans, E.C., Damsté, J.S.S., 2007. Environmental controls on bacterial tetraether membrane lipid distribution in soils. Geochim. Cosmochim. Acta. 71, 703-713.

Williams, A.E., Rodoni, D.P., 1997. Regional isotope effects and application to hydrologic investigations in southwestern California. Water Resour. Res. 33, 1721-1729.

Williams, A.P, Allen, C.D., Macalady, A.K., Griffin, D., Woodhouse, C.A., Meko, D.M., Swetnam, T.W., Rauscher, S.A., Seager, R., Grissino-Mayer, H.D., Dean, J.S., Cook, E.R., Gangodagamage, C., Cai, M., McDowell, N.G., 2012. Temperature as a potent driver of regional forest drought stress and tree mortality. Nat. Clim. Chang. 3, 292, doi: 10.1038/NCLIMATE1693.

Wong, C.I., Potter, G.L., Montañez, I.P., Otto-Bliesner, B.L., Behling, P., Oster, J.L., 2016. Evolution of moisture transport to the western US during the last deglaciation. Geophys. Res. Lett., doi:10.1002/2016GL068389.

Figure and Table Captions

Figure 1: A. Map of study region with location of Lake Elsinore (red star) and other paleoclimate archives discussed in the text (yellow stars) including their age range. The arrows represent two distinct storm trajectories carrying moistures of different isotopic compositions towards the western US. B. Lake Elsinore catchment (red boundary) and topography; Lake Elsinore catchment is part of the larger catchment of Santa Ana River (black boundary) which flows into the North Pacific. Red diamonds show the locations of river sampling on the San Jacinto River (SJR). Dashed line denotes transect in c. C. Profile of elevation across a transect from Lake Elsinore to Mt. San Jacinto (Mt. SJ), with distribution of vegetation types and elevations of river sampling (red diamonds).

Figure 2: Multi-proxy reconstruction for Lake Elsinore. A. Plant wax δD (black), and $\delta^{13}C_{wax}$ (green). B. BrGDGT estimates of temperature (blue) and ACE index for salinity (grey). C. Pollen evidence for warmer and drier conditions showing oak (*Quercus*, black) and dry (xeric) taxa (Amaranthaceae, Asteraceae and *Artemisia*, pink; Heusser et al., 2015). D. Showing sand evidence for runoff (Kirby et al., 2018) and cooler and wetter conditions, juniper (Cupressaceae; Heusser et al., 2015). Blue shading denotes consistently cold and wet conditions, all other times are warm, dry or variable. Yellow shading denotes extremely dry conditions in the catchment from 27.5 – 25.5 ka based on pollen (Heusser et al., 2015) and sandy sediments indicating when Lake Elsinore was 3.2 – 4.5 m deep, about half modern depth (Kirby et al., 2018).

Figure 3: Comparison of paleoprecipitation δD values reconstructed from Lake Elsinore δD_{wax} including ice volume correction (black circles, this study; white circles, Kirby et al., 2013), and Zaca Lake δD_{wax} (gray; Feakins et al., 2014), uncertainties associated with calibration are 5‰

692 (not graphed), alongside speleothem $\delta^{18}O$ calcite records from the Leviathan Cave (gold), and
693 Pinnacle Cave (orange) Nevada (including ice volume correction and adjusted to align into a
694 single location equivalent record, the Leviathan Chronology; Lachniet et al., 2014, Lachniet,
695 2016), with the second y-axis scaled x8 to enable direct comparison.

696 **Figure 4:** Comparison of late glacial and deglacial temperatures in southern California: blue -
697 from the MBT'_{5me} index of brGDGTs in Lake Elsinore (this study) using the calibration of
698 Russell et al. (2018); pink - from Mg/Ca in *G. bulloides* from ODP Site 1017E in the Santa
699 Barbara Basin (Pak et al., 2012); light blue - from alkenone-derived $U^{k}_{37}{}'$ (Seki et al., 2002). For
700 global temperature context, showing the European Project for Ice Coring in Antarctica (EPICA)
701 pCO_2 composite record (< 22 ka from Dome C and >22 ka from Vostok) showing gradual change
702 associated with global warming across the glacial termination (Monnin et al., 2001, Petit et al.,
703 1999). In contrast, North Greenland Ice Core Project NGRIP $\delta^{18}O$ data (North Greenland Ice
704 Core Project, 2004) with abrupt features of late glacial North Atlantic millennial scale climate
705 variability annotated.

706

707

Table 1: River samples from Lake Elsinore catchment (additional data reported in Appendix A).

ID	Lat.	Long.	Elevat-ion (m)	δD_{wax} (‰)	σ (‰)	δD_w (‰)	σ (‰)	$\delta^{18}O_w$ (‰)	σ (‰)	$\varepsilon_{wax/w}$ (‰)	c. σ[a] (‰)
SJR 1	33.736	-116.824	615	-152	2	-71.6	0.5	-10.2	0.2		
SJR 2	33.736	-116.816	630	-151	4	-72.2	1	-10.2	0.2		
Mean (SJR 1&2)				**-151**	**5**	**-71.9**	**1.1**	**-10.2**	**0.3**	**-86**	**5**
SJR 3	33.741	-116.718	1630	n.a.	n.a.	-73.7	0.4	-11.9	0.1		

[a] Combined 1σ uncertainty

708

Figure 1

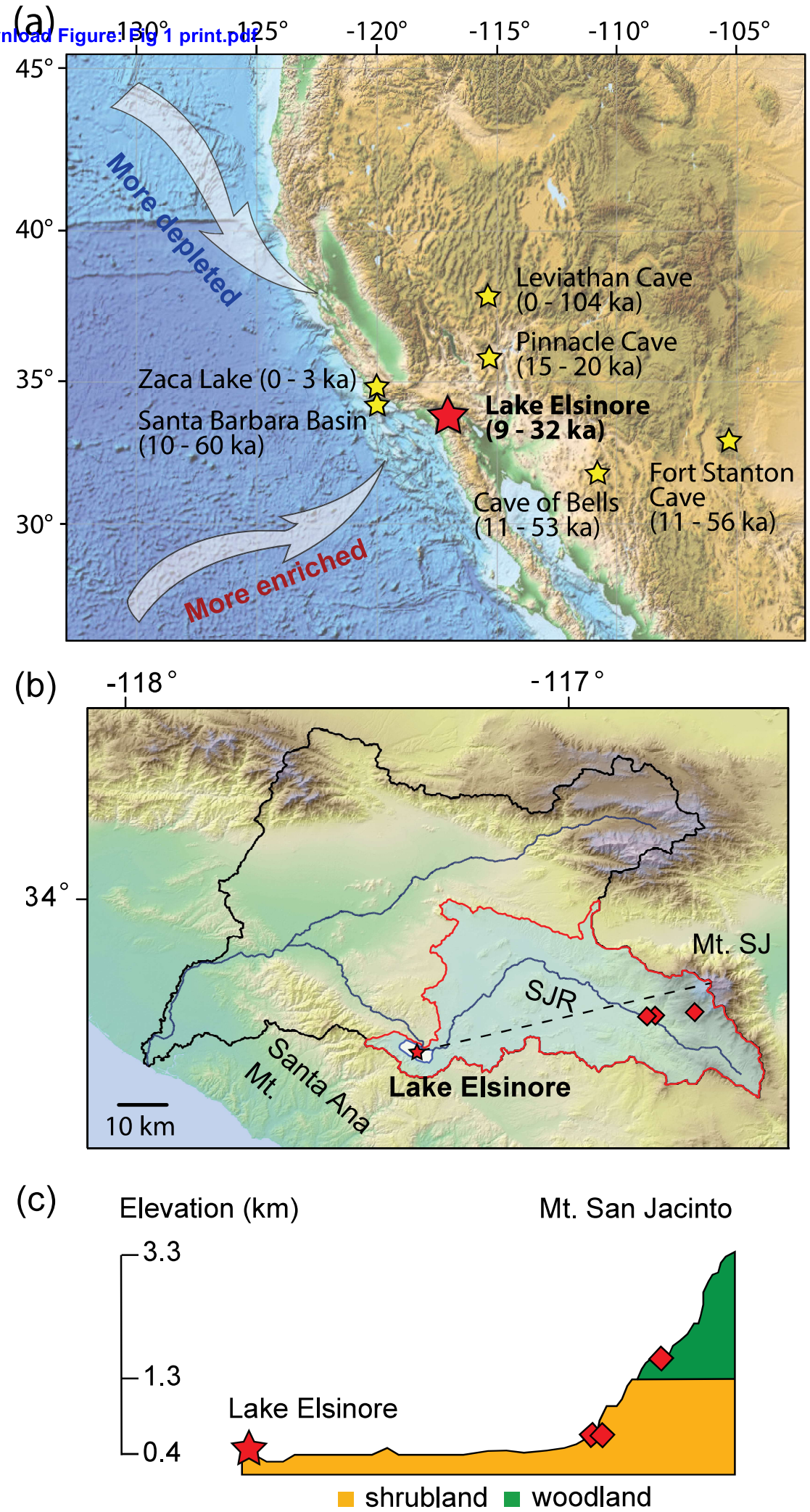

Figure 2

Click here to download Figure: Fig 2 v6.pdf

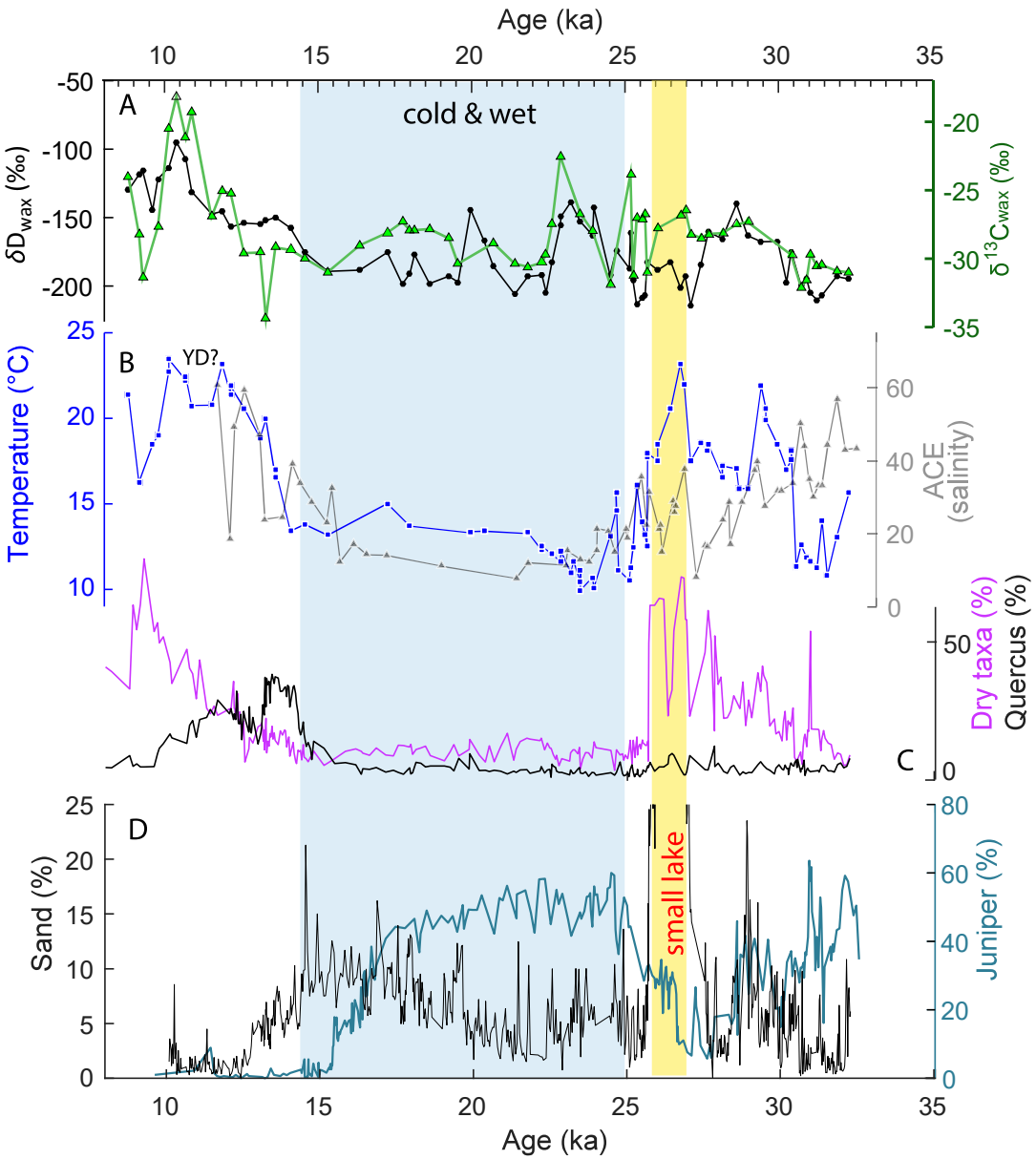

Figure 3

Click here to download Figure: Fig 3.pdf

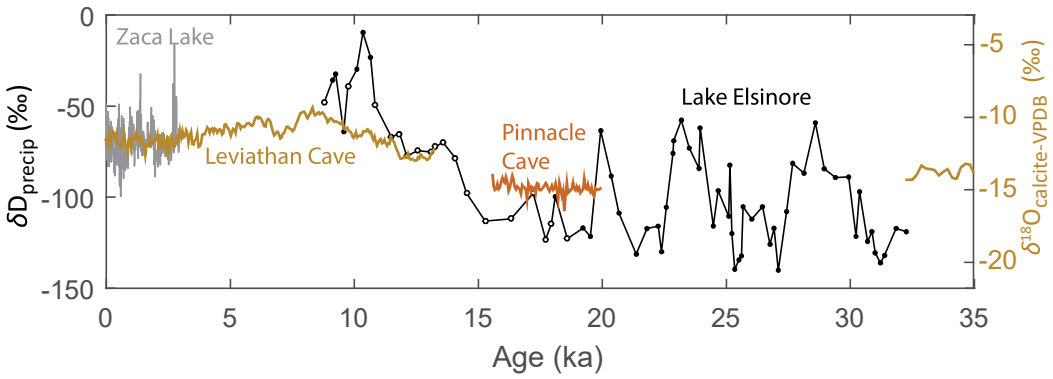

Figure 4

Click here to download Figure: Fig 4.pdf

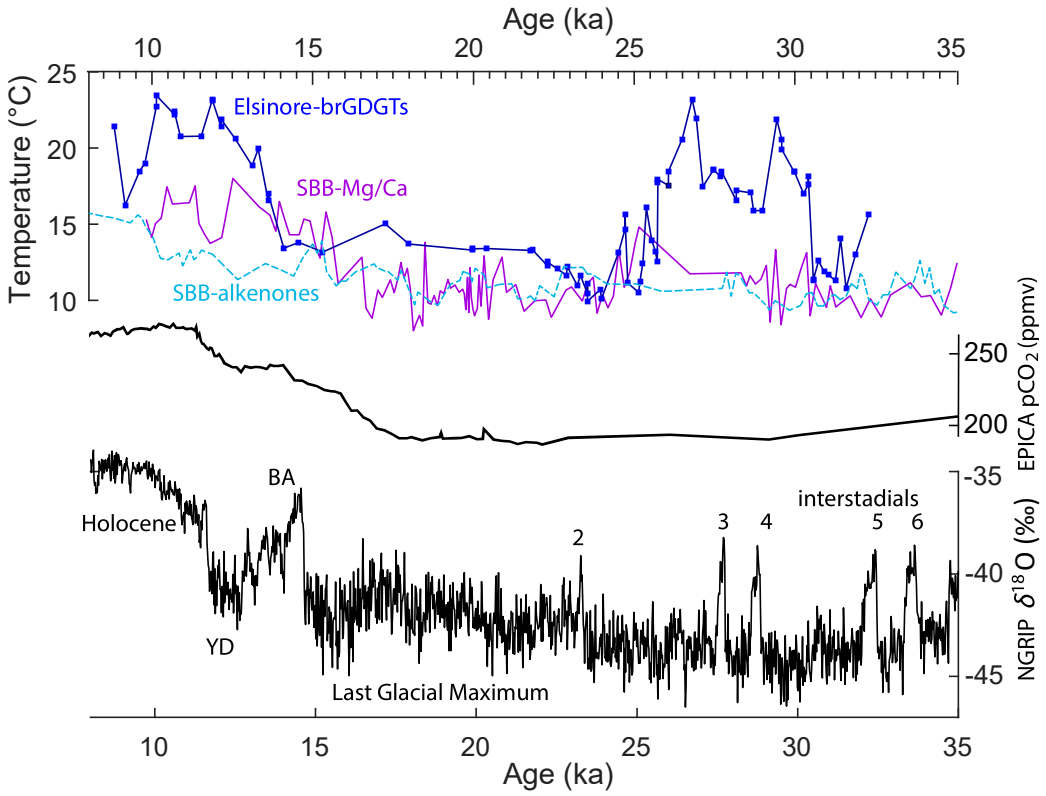

Supplementary material for online publication only

Click here to download Supplementary material for online publication only: Elsinore_AppendixA_2019-01-22.xlsx